



Cite this: DOI: 10.1039/c9tc05548g

Effect of large work function modulation of MoS₂ by controllable chlorine doping using a remote plasma†

Ki Hyun Kim,^a Ki Seok Kim,^{ab} You Jin Ji,^a Inyong Moon,^c Keun Heo,^d
Dong-Ho Kang,^d Kyong Nam Kim,^e Won Jong Yoo,^{id} Jin-Hong Park^{id} and
Geun Young Yeom^{id} *^{ac}

Adjusting the intrinsic properties of 2-dimensional (2D) transition metal dichalcogenide materials is important for their various applications in electronic devices. Among them, molybdenum disulfide (MoS₂) is one of the most attractive layered 2D materials because of its excellent electrical properties as well as good thermal and oxidation stability. Controlling the doping process and analyzing how the dopant atoms affect the device properties are crucial for advanced applications of TMDs. In this study, a simple and controllable chlorine doping method of MoS₂ using a remote inductively coupled plasma (ICP) was studied and the effect of doping on the properties of MoS₂ was investigated by adjusting the work function of MoS₂. Kelvin probe force microscopy (KPFM) shows a gradual decrease of the work function with increasing chlorine radical treatment time. Chlorine doped MoS₂ field effect transistors (FETs) exhibited improved electrical characteristics such as the field effect mobility and on current level as demonstrated by the transfer characteristics (I_d - V_{gs}). Especially, the chlorine doped MoS₂ FETs showed increased photoresponsivity by 1.94 times (from 424 to 824 A W⁻¹) for green light (λ = 520 nm) and, much more interestingly, 8.59 times (from 37.6 to 323 A W⁻¹) for near-infrared (NIR) light (λ = 785 nm).

Received 10th October 2019,
Accepted 7th December 2019

DOI: 10.1039/c9tc05548g

rsc.li/materials-c

Introduction

Molybdenum disulfide (MoS₂) has attracted widespread interest due to its unique and adjustable electrical and optical properties such as high field effect mobility and tunable optical band gap.¹⁻⁴ With a two-dimensional structure composed of S-Mo-S in-plane covalent bonding and van der Waals interaction between two adjacent layers, monolayer MoS₂ shows a 1.9 eV direct band-gap and 1.29 eV indirect band-gap for bulk MoS₂.⁵⁻⁷ The excellent and controllable electrical properties of MoS₂ allow electronic applications such as field effect transistors and

phototransistors.^{8,9} To utilize these unique properties of MoS₂ in various semiconductor devices, modifications of MoS₂ layers such as thickness control and p-(n)-type doping processes are required. Doping is one of the most effectively used techniques in controlling the semiconducting properties for advanced applications of MoS₂ due to the fact that dopants generally govern the chemical and electrical properties of materials, especially for 2-dimensional atomically thin semiconductors. Furthermore, by changing the electronic structure of MoS₂ with proper doping, the intrinsic electrical and optical properties could be improved.¹⁰⁻¹⁴ Until now, many studies on the doping of MoS₂ can be found for various applications of MoS₂. For example, by chlorine doping with a dichloroethane (DCE) solution process, the mobility and contact resistance of MoS₂ were controlled.¹⁵ In addition, through the doping of rhenium (Re) on a MoS₂ film by incorporating a Re layer between the Mo layers during the MoS₂ synthesis stage, controllability of the resistivity and Hall coefficient of MoS₂ was achieved.¹⁶ The optical properties of MoS₂ were also adjusted by doping of a monolayer-MoS₂ film through lithium (Li) evaporation.¹⁷ In addition to the above doping strategies, the doping of MoS₂ with AuCl₃ (p-type), benzyl viologen (BV) (n-type), Au nanoparticles (p-type), *etc.* has been investigated to fabricate low-power operating photodevices having a p-n structure.¹⁸⁻²¹

^a Department of Advanced Materials Science and Engineering, Sungkyunkwan University, 2066 Seobu-ro, Jangan-gu, Suwon-si, Gyeonggi-do 16419, Republic of Korea

^b Research Laboratory of Electronics, Massachusetts Institute of Technology, Cambridge, MA, USA

^c SKKU Advanced Institute of Nano Technology (SAINT), Sungkyunkwan University, 2066 Seobu-ro, Jangan-gu, Suwon-si, Gyeonggi-do 16419, Republic of Korea. E-mail: gyyeom@skku.edu

^d School of Electronic and Electrical Engineering, Sungkyunkwan University, 2066 Seobu-ro, Jangan-gu, Suwon-si, Gyeonggi-do 16419, Republic of Korea

^e School of Advanced Materials Science and Engineering, Daejeon University, Yongun-dong, Dong-gu, Daejeon 34520, Korea. E-mail: knam1004@skku.edu

† Electronic supplementary information (ESI) available. See DOI: 10.1039/c9tc05548g

Even though many different dopant materials and methods have been investigated for the doping of 2D MoS₂, fast and precise doping with minimized damage to MoS₂ could be quite challenging. For example, the doping of MoS₂ achieved during the MoS₂ synthesis stage and through the evaporation of dopant atoms may cause structural distortion of MoS₂. Doping of MoS₂ can be achieved effectively without damage by wet doping such as with chlorine using a 1,2-dichloroethane (DCE) solution. However, this wet doping method requires a relatively long process time of over 12 hours.¹⁵ Therefore, a dry doping process which can realize fast and precise doping with minimization of damage to MoS₂ is required for the further applications of MoS₂.

Here, we report an effective method for precise dry doping of MoS₂ by controlled chlorine radicals generated using a remote plasma system. Our doping method gives advantages over previous doping methods such as doping during synthesis, solution-based wet doping methods, *etc.* in that the remote plasma doping can effectively control the dopant amount in MoS₂ without damaging the surface and with high throughput over a large area substrate.

Results and discussion

Using first principles calculations, the variation of the electronic band structure and the change of binding energies by chlorine doping on MoS₂ have been investigated. Fig. 1 shows the change of the MoS₂ band structures by two different doping routes of MoS₂: surface adsorption on MoS₂ (Fig. 1a) and adsorption on sulfur vacancies in MoS₂ (Fig. 1b). To investigate

the interaction between chlorine and pristine MoS₂ (surface adsorption) as well as MoS₂ and sulfur vacancies (adsorption on sulfur vacancies), the adsorption energy of a chlorine atom was calculated using the equation below:

$$E(\text{adsorption}) = E(\text{substrate-Cl}) - E(\text{substrate}) - E(\text{Cl})$$

where, $E(\text{substrate-Cl})$ corresponds to the total energy of the system with the Cl adsorbed on MoS₂ (either pristine or with a sulfur vacancy), $E(\text{substrate})$ is the energy of MoS₂ (either pristine or with a sulfur vacancy), and $E(\text{Cl})$ is the energy of a free chlorine atom. As illustrated in Fig. 1a, the calculated band structure for the pristine trilayer MoS₂ shows the characteristic indirect band gap of the MoS₂ system, having a band gap within 1.3 eV estimated from the band structure in Fig. 1a. A direct bandgap showing the *K* point in the band structure is observed when the thickness of MoS₂ is thinned down to a monolayer.^{6,22} Upon adsorption of chlorine on the S-top of pristine MoS₂, a notable change in the band structure is the appearance of a new band leading to a lower band gap of 0.38 eV. The calculated $E_{\text{adsorption}}$ shows that this process is a favorable one leading to a change in energy by -0.9 eV upon chlorine adsorption. In addition to the adsorption of a chlorine atom on the pristine MoS₂ surface, there is another possible binding state of chlorine on the MoS₂ system where a chlorine atom is adsorbed on a sulfur atom vacancy site. As shown in the band structure for MoS₂ in Fig. 1b, when the top MoS₂ layer has a sulfur vacancy, there is a decrease in the band gap by 0.4 eV (from 1.3 eV to 0.9 eV). After the chlorine atom is adsorbed on the sulfur vacancy, the Fermi level moves close to the conduction band. This upward shift of the Fermi level is characteristic of n-doping.

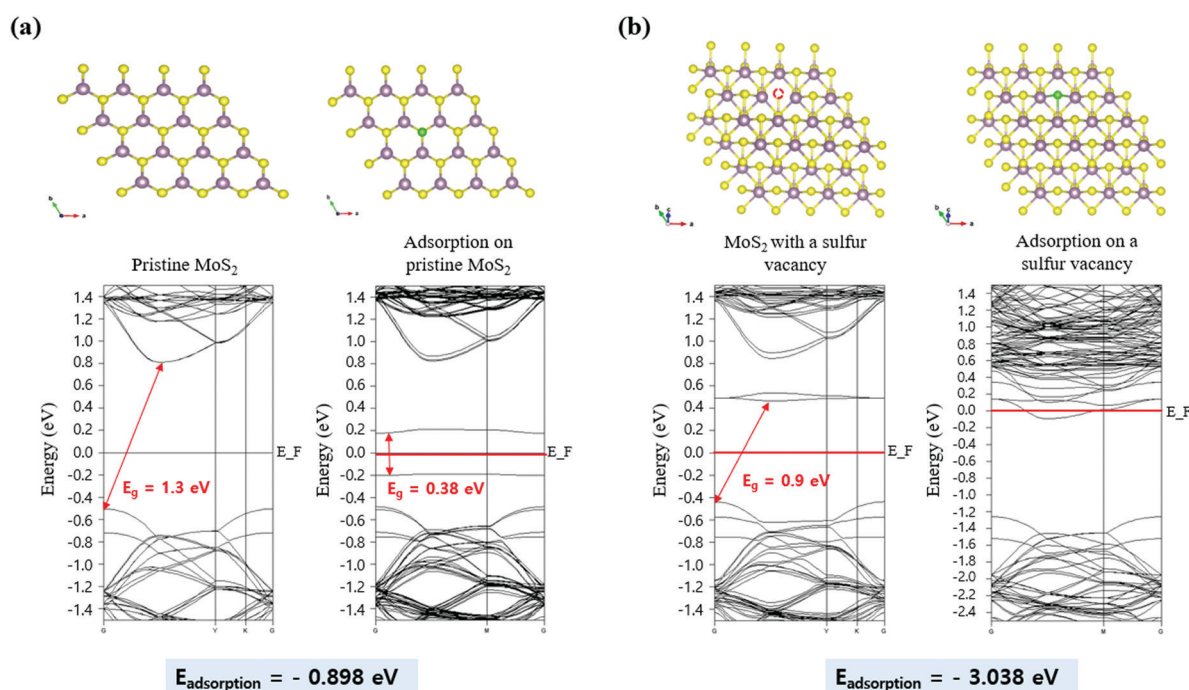


Fig. 1 Change of band structure for (a) adsorption of a chlorine atom on pristine MoS₂ and (b) adsorption of a chlorine atom on a S vacancy site of MoS₂.

Hence, based on first principles calculations, it was confirmed that the adsorption of a Cl atom on the sulfur vacancy site leads to an effect of n-type doping.

Fig. 2a shows the Raman spectra of the trilayer MoS₂ flakes used in this research. They showed a 23.4 cm⁻¹ frequency difference between A_{1g} and E_{2g}¹, having good agreement with previous research on the relationship between the number of MoS₂ layers and the gap between the two peaks.^{23,24} After treatment with a remote chlorine plasma for 30 s, the position and intensity of the A_{1g} and E_{2g}¹ peaks are barely changed, indicating that the chlorine atoms were doped in the lattice without causing any thickness change or noticeable distortion of the nearby lattice (crystallinity). The MoS₂ layer thickness measured by atomic force microscopy (AFM) also reveals that the chlorine radical treatment doesn't cause layer thinning of the MoS₂ flake (Fig. S2, ESI[†]). To ascertain whether chlorine atoms are incorporated in the MoS₂ lattice or not, XPS analysis was conducted. The presence of chlorine atoms on the MoS₂ surface after the treatment could be confirmed by the appearance of the Cl 2p peak in Fig. 2b. At the same time, as shown in Fig. 2c and d, the peaks at 232.7/229 eV for Mo 3d and 163.6/162.5 eV for S 2p were blue-shifted to 233.2/230.1 eV for Mo 3d and to 164/162.9 eV for S 2p (shifted by 0.4–0.5 eV). The shifts of the binding energy of the Mo 3d and S 2p peaks are shown in Fig. 2e. This shift toward higher binding energy is characteristic of an n-type doping effect which is caused by a Fermi level increase by n-type chlorine dopants.^{15,25} A higher blue-shift of the Mo 3d peaks was observed for CVD MoS₂ having a lower initial S/Mo ratio below 2 (Fig. S5, ESI[†]). Fig. 2f shows the relative atomic percentage of chlorine atoms and the S/Mo ratio of the MoS₂ flake with the chlorine radical treatment time. The chlorine concentration increases as the treatment time increases, and then saturated after 30 s. In addition, during the process,

there was no significant deviation of the S/Mo ratio from the stoichiometry of MoS₂. Moreover, as shown in Fig. 2c, the relative intensity of the S–Mo–S binding peak at ~227 eV and the Mo⁶⁺ peak at ~236 eV didn't change noticeably after chlorine doping. These two peaks (S–Mo–S and Mo⁶⁺) are found to be related to the crystallinity of the MoS₂ lattice according to our previous research: the removal of top sulfur by ion bombardment leads to formation of defective sulfur sites in the MoS₂ lattice and this structural disorder of the MoS₂ lattice causes the decrease of the S–Mo–S intensity at ~227 eV and the emergence of Mo⁶⁺ at ~236 eV at the same time.²⁵ Consequently, the above results indicate that there was no damage during the chlorine doping process.

To investigate the effect of chlorine doping on the work function of MoS₂, a KPFM measurement was conducted. A KPFM probe was calibrated with highly oriented pyrolytic graphite (HOPG), which is a reference material having a work function of 4.6 eV, to measure the absolute work function of MoS₂. Fig. 3a and b show the work function mapping of pristine and chlorine-doped MoS₂ flakes, respectively, after exposure to a remote chlorine plasma for 30 s. The bright image of the MoS₂ surface in Fig. 3a, which shows a relatively low Fermi level with a high work function, turned a dark color (Fig. 3b) indicating an increased Fermi level (lowered work function) of the MoS₂ flake by n-type chlorine doping. The dark color of the doped MoS₂ was relatively uniform, possibly due to the uniform doping of chlorine on the MoS₂ surface as supported by the EDS analysis (Fig. S3, ESI[†]). As shown in Fig. 3c, the work function of the MoS₂ flakes decreased gradually (shifted toward n-type) from 4.6 to below 4.3 eV with increasing the treatment time from 0 to 30 s and saturated at ~30 s. This tendency is important in device operation because the work function of MoS₂ gets close to that of Ti (~4.33 eV)²⁶ after chlorine doping.

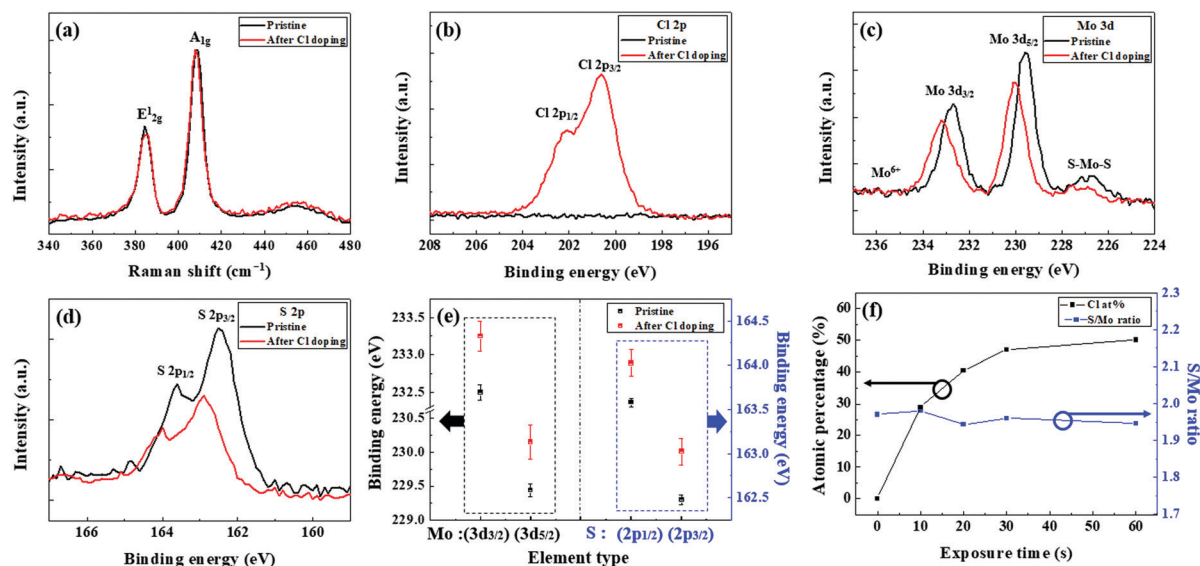


Fig. 2 (a) Raman spectra of trilayer MoS₂ flakes before and after Cl radical treatment. Narrow scan XPS data of (b) Cl 2p, (c) Mo 3d, and (d) S 2p measured before and after Cl radical treatment. (e) Binding energy shift of Mo 3d and S 2p. (f) Relative at% of chlorine atoms and S/Mo ratio during the process measured from 0 to 60 s.

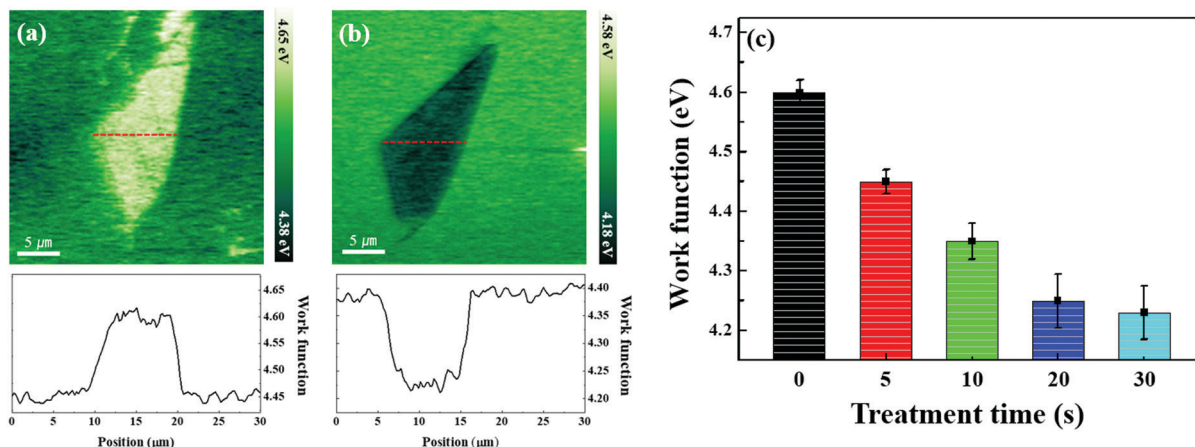


Fig. 3 Work function mapping of MoS₂ (a) before and (b) after chlorine doping (for 30 s). The brighter image denotes a higher work function of MoS₂. (c) Work function of MoS₂ flakes with increasing chlorine radical treatment time.

The tendency in the saturation of the work function was similar to the XPS results on the chlorine atomic percentage in Fig. 2f, where the chlorine atomic percentage increased gradually with increasing chlorine treatment time and saturated at around 30 s.

Back gated MoS₂ FETs were fabricated with pristine and chlorine doped MoS₂ and the current–voltage characteristics of these MoS₂ FETs were measured in dark and illuminated

conditions after chlorine treatment for 30 s. As shown in Fig. 4a, after chlorine doping, the n-type property of MoS₂ was enhanced as the work function of MoS₂ gets close to that of Ti as confirmed by the previous KPFM results. Fig. 4b and c show the change of the field effect mobility, on current level, and threshold voltage measured for five MoS₂ FETs (S1–S5) before and after doping for 30 s. The additional electrons supplied by

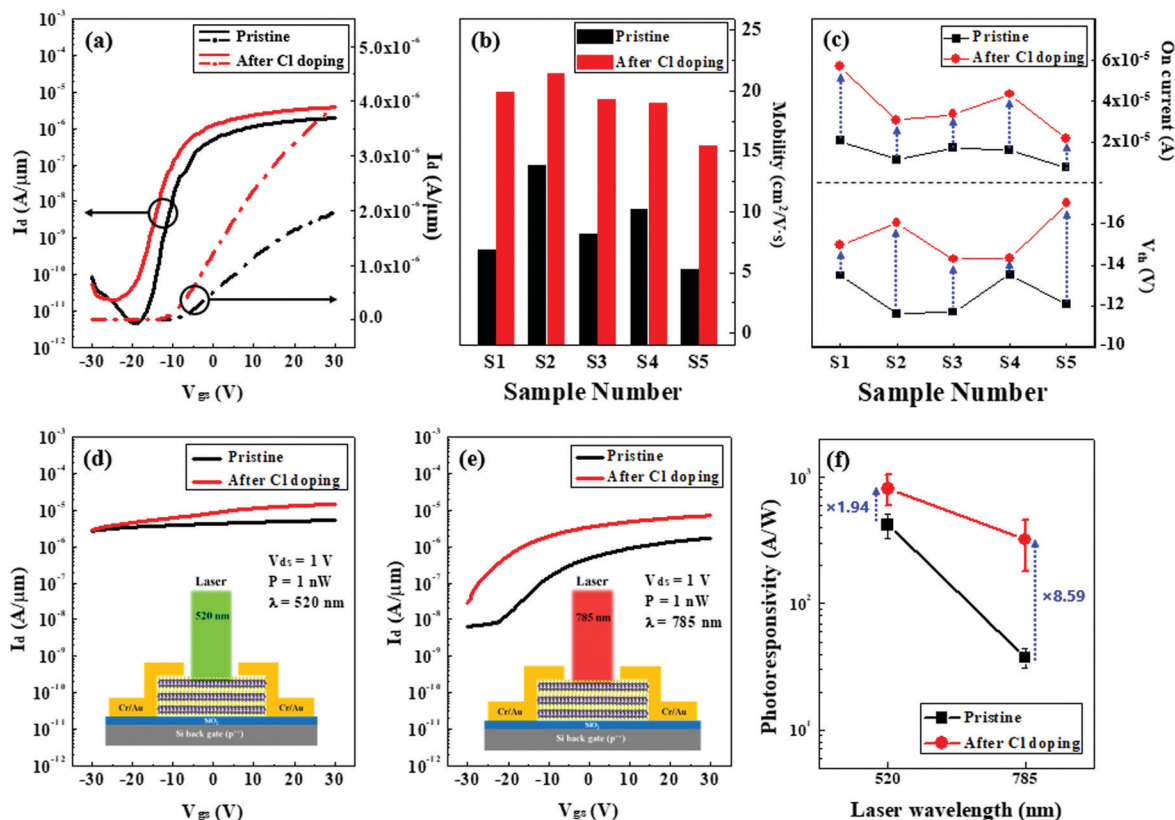


Fig. 4 (a) Transfer characteristics of MoS₂ FETs in the dark state. The left and right curves denote log and linear scales respectively. Variations of the (b) mobility, (c) on current and threshold voltage (V_{th}) of MoS₂ FETs (for 5 different samples). Transfer curves of MoS₂ FETs under illumination with a (d) green (520 nm) laser, and (e) NIR (785 nm) laser. (f) Comparison of the photoresponsivity between pristine and chlorine doped MoS₂ for 520 and 785 nm lasers. The treatment time for chlorine doped MoS₂ was 30 s.

chlorine atoms to MoS₂ by the doping contribute to enhancement of the on-current level as well as the field effect mobility while changing the threshold voltage toward the negative voltage direction (even though there is some deviation among the devices). Fig. 4d and e are the transfer characteristics of the MoS₂ FETs under illumination with a green ($\lambda = 520$ nm) laser, and a NIR ($\lambda = 785$ nm) laser, respectively. As shown in Fig. 4d, after chlorine doping, there was an increase of photoresponsivity from 424 to 824 A W⁻¹ (1.94 times enhancement at $V_{gs} = 0$ V) for $\lambda = 520$ nm. For $\lambda = 785$ nm, the MoS₂ FETs showed lower photoresponsivity (for pristine MoS₂, ~ 37.6 A W⁻¹) compared with the responsivity at $\lambda = 520$ nm (424 A W⁻¹), but much higher photoresponsivity than that of the pristine MoS₂ FET was observed after chlorine doping (from 37.6 to 323 A W⁻¹, 8.59 times enhancement, Fig. 4e). The calculated photoresponsivity of pristine and chlorine doped MoS₂ FETs illuminated with 520 and 785 nm lasers is illustrated in Fig. 4f. This can be explained by the increase of the Fermi level of MoS₂: the pristine MoS₂ FET generates insufficient photocurrent with illumination with NIR, resulting in low photoresponsivity, but a significant amount of photocarriers can be generated when the Fermi level of MoS₂ is increased by chlorine doping. The difference in the photoresponsivity before and after chlorine doping for a gate bias voltage V_{gs} (-30 to $+30$ V) is calculated (Fig. S4, ESI[†]).

In general, as the gate voltage V_{gs} increases, the effective barrier height between the electrode and MoS₂ decreases, and the contact resistance also decreases.²⁷ Therefore, the photoresponsivity increases and the difference between before and after the chlorine doping becomes more noticeable. That is, the enhanced photoresponsivity of the chlorine doped MoS₂ FETs can be explained with a closer Fermi level to the conduction band minimum of MoS₂ by n-type doping and this effect is much more noticeable in the NIR region than the visible region because MoS₂ photodetectors usually respond well in the visible (especially at short wavelengths) region even in the intrinsic state but weakly respond in the infrared region.^{28–31} Therefore, the enhanced photoresponsivity of the chlorine doped MoS₂ photodetector obtained in this study can be very useful in various optoelectronic applications.

Experimental section

Preparation of MoS₂ flakes and device fabrication

In this research, material characterization and evaluation of device properties were accomplished using bi-/tri-layer-MoS₂ flakes. The MoS₂ flakes were transferred to a ~ 300 nm-thick silicon dioxide substrate using a conventional mechanical exfoliation method using 3 M tape.³² The MoS₂ field effect transistors (FETs) were fabricated by a photolithography process (AZ5214E photoresist and AZ MIF 300 developer) with the trilayer MoS₂ flakes on highly p-type doped Si/SiO₂ wafers acting as a back-gate, followed by the deposition of electrodes (Ti 5 nm/Au 50 nm) by an electron-beam evaporation process. The channel width and length of all MoS₂ FETs used in this study were 10 and 10 μm , respectively.

Doping of MoS₂ with chlorine

The chlorine doping was carried out using a radio frequency (rf, 13.56 MHz) inductively coupled plasma (ICP) system. To protect the MoS₂ from bombardment by electrons and ions, as a remote plasma source, a double-layer mesh grid was installed below the ICP source allowing only radicals and molecules to pass through. The schematic drawing of the remote ICP system with the mesh grid used in this experiment can be found in Fig. S1 (ESI[†]). During the process, the pressure and gas flow rate were maintained at 10 mTorr and 80 sccm, respectively, and 18 W rf source power was applied to the ICP electrode.

Material and device characterization

The thickness of the MoS₂ flakes was assessed by Raman spectroscopy (WITEC alpha 300 M[†]) with a center wavelength of 532 nm. For precise analysis during the experiment, the laser power was kept at 2.5 mW, which is carefully adjusted to avoid heating damage to MoS₂. The chemical composition and binding state of MoS₂ were characterized by X-ray photoelectron spectroscopy (XPS, MultiLab 2000, Thermo VG, Mg K α source) after calibration with C 1s at 284.5 eV. The surface distribution of chlorine atoms after the treatment was observed using an energy dispersive spectroscopy (EDS) accessory with a transmission electron microscope (TEM, Analytic STEM; JEM-2100F). The work function was calculated by measuring the surface potential of the MoS₂ flakes using a Kelvin probe force microscope (KPFM) using a common method of $V_{CPD} = \phi_{\text{sample}} - \phi_{\text{tip}}$, where V_{CPD} is the charge potential difference between the sample (MoS₂) and the tip, ϕ_{sample} is the surface potential of MoS₂, and ϕ_{tip} is the potential of the KPFM tip.³³ The evaluation of the MoS₂ FETs was performed with a probe station (M6VC, MSTECH) in ambient conditions with illumination with a laser using a semiconductor analyzer (Agilent 4155C). Photoresponsivity (R) was calculated as the photocurrent (I_{photo}) divided by the incident laser power (P_{laser}) and the power of the laser was adjusted to 1 nW. Here, all drain currents (I_d) were normalized by the channel width (10 μm). The theoretical investigation of the electronic structure of MoS₂ before and after chlorine doping of MoS₂ was conducted through an ab initio simulation package after calculating the lattice constant and bond length of MoS₂ as 3.213 and 2.436 Å, respectively. More details about the calculation method can be found in previous studies.^{25,34}

Conclusions

The effects of chlorine doping on few layer (2–3 layers) MoS₂ were investigated. Fast and uniform chlorine doping of MoS₂ could be achieved by a chlorine in a remote plasma type ICP system. The XPS and KPFM measurements confirmed that the concentration of chlorine atoms increases gradually with increasing plasma exposure time, causing an increase of the Fermi level (closer to the conduction band minimum) and, consequently, a gradual shift in the MoS₂ work-function of ~ 0.4 eV until saturation by the plasma treatment after 30 s. Finally, photocurrent measurements showed the increased

photocurrent of MoS₂ FETs by chlorine doping under two illumination conditions ($\lambda = 520$ and 785 nm). However, a much more enhanced photoresponsivity rate was observed in the NIR (from 37.6 to 323 A W⁻¹, an 8.59 times increase at $\lambda = 785$ nm) than in the visible region (from 424 to 824 A W⁻¹, a 1.94 times increase at $\lambda = 520$ nm) after chlorine doping.

Conflicts of interest

There are no conflicts to declare.

Acknowledgements

This work was supported by the Nano-Material Technology Development Program through the National Research Foundation of Korea (NRF), funded by the Ministry of Education, Science and Technology (2016M3A7B4910429). This research was also supported by the Basic Science Research Program through the National Research Foundation of Korea (NRF) funded by the Ministry of Education (2019R1I1A1A01044096).

References

- B. Radisavljevic, A. Radenovic, J. Brivio, V. Giacometti and A. Kis, *Nat. Nanotechnol.*, 2011, **6**, 147–150.
- A. Pezeshki, S. H. Hosseini Shokouh, S. R. A. Raza, J. S. Kim, S. W. Min, I. Shackery, S. C. Jun and S. Im, *J. Mater. Chem. C*, 2014, **2**, 8023–8028.
- H. J. Conley, B. Wang, J. I. Ziegler, R. F. Haglund, S. T. Pantelides and K. I. Bolotin, *Nano Lett.*, 2013, **13**, 3626–3630.
- S. Mouri, Y. Miyauchi and K. Matsuda, *Nano Lett.*, 2013, **13**, 5944–5948.
- G. Eda, H. Yamaguchi, D. Voiry, T. Fujita, M. Chen and M. Chhowalla, *Nano Lett.*, 2011, **11**, 5111–5116.
- A. Splendiani, L. Sun, Y. Zhang, T. Li, J. Kim, C. Y. Chim, G. Galli and F. Wang, *Nano Lett.*, 2010, **10**, 1271–1275.
- K. F. Mak, C. Lee, J. Hone, J. Shan and T. F. Heinz, *Phys. Rev. Lett.*, 2010, **105**, 136805.
- Z. Yin, H. Li, H. Li, L. Jiang, Y. Shi, Y. Sun, G. Lu, Q. Zhang, X. Chen and H. Zhang, *ACS Nano*, 2011, **6**, 74–80.
- M. Buscema, M. Barkelid, V. Zwiller, H. S. J. Van Der Zant, G. A. Steele and A. Castellanos-Gomez, *Nano Lett.*, 2013, **13**, 358–363.
- H. P. Komsa, J. Kotakoski, S. Kurasch, O. Lehtinen, U. Kaiser and A. V. Krasheninnikov, *Phys. Rev. Lett.*, 2012, **109**, 035503.
- Y. C. Lin, D. O. Dumcenco, H. P. Komsa, Y. Niimi, A. V. Krasheninnikov, Y. S. Huang and K. Suenaga, *Adv. Mater.*, 2014, **26**, 2857–2861.
- K. Zhang, S. Feng, J. Wang, A. Azcatl, N. Lu, R. Addou, N. Wang, C. Zhou, J. Lerach, V. Bojan, M. J. Kim, L. Q. Chen, R. M. Wallace, M. Terrones, J. Zhu and J. A. Robinson, *Nano Lett.*, 2015, **15**, 6586–6591.
- S. McDonnell, R. Addou, C. Buie, R. M. Wallace and C. L. Hinkle, *ACS Nano*, 2014, **8**, 2880–2888.
- J. Suh, T. E. Park, D. Y. Lin, D. Fu, J. Park, H. J. Jung, Y. Chen, C. Ko, C. Jang, Y. Sun, R. Sinclair, J. Chang, S. Tongay and J. Wu, *Nano Lett.*, 2014, **14**, 6976–6982.
- L. Yang, K. Majumdar, H. Liu, Y. Du, H. Wu, M. Hatzistergos, P. Y. Hung, R. Tieckelmann, W. Tsai, C. Hobbs and P. D. Ye, *Nano Lett.*, 2014, **14**, 6275–6280.
- T. Hallam, S. Monaghan, F. Gity, L. Ansari, M. Schmidt, C. Downing, C. P. Cullen, V. Nicolosi, P. K. Hurley and G. S. Duesberg, *Appl. Phys. Lett.*, 2017, **111**, 203101.
- N. Saigal, I. Wielert, D. Capeta, N. Vujičić, B. V. Senkovskiy, M. Hell, M. Kralj and A. Grüneis, *Appl. Phys. Lett.*, 2018, **112**, 121902.
- M. S. Choi, D. Qu, D. Lee, X. Liu, K. Watanabe, T. Taniguchi and W. J. Yoo, *ACS Nano*, 2014, **8**, 9332–9340.
- K. P. Dhakal, D. L. Duong, J. Lee, H. Nam, M. Kim, M. Kan, Y. H. Lee and J. Kim, *Nanoscale*, 2014, **6**, 13028–13035.
- H. M. Li, D. Lee, D. Qu, X. Liu, J. Ryu, A. Seabaugh and W. J. Yoo, *Nat. Commun.*, 2015, **6**, 6564.
- J. Chao, M. Zou, C. Zhang, H. Sun, D. Pan, H. Pei, S. Su, L. Yuwen, C. Fan and L. Wang, *Nanotechnology*, 2015, **26**, 274005.
- S. Ahmad and S. Mukherjee, *Graphene*, 2014, **3**, 52.
- H. Li, Q. Zhang, C. C. R. Yap, B. K. Tay, T. H. T. Edwin, A. Olivier and D. Baillargeat, *Adv. Funct. Mater.*, 2012, **22**, 1385–1390.
- F. Mos, C. Lee, H. Yan, L. E. Brus, T. F. Heinz, K. J. Hone and S. Ryu, *ACS Nano*, 2010, **4**, 2695–2700.
- K. S. Kim, K. H. Kim, Y. Nam, J. Jeon, S. Yim, E. Singh, J. Y. Lee, S. J. Lee, Y. S. Jung, G. Y. Yeom and D. W. Kim, *ACS Appl. Mater. Interfaces*, 2017, **9**, 11967–11976.
- D. R. Lide, *Handbook of Chemistry and Physics*, CRC Press, 1st edn, 1988, p. 69.
- W. Bao, X. Cai, D. Kim, K. Sridhara and M. S. Fuhrer, *Appl. Phys. Lett.*, 2013, **102**, 042104.
- O. Lopez-Sanchez, D. Lembke, M. Kayci, A. Radenovic and A. Kis, *Nat. Nanotechnol.*, 2013, **8**, 497.
- J. K. Ellis, M. J. Lucero and G. E. Scuseria, *Appl. Phys. Lett.*, 2011, **99**, 261908.
- S.-H. Jo, H.-Y. Park, D.-H. Kang, J. Shim, J. Jeon, S. Choi, M. Kim, Y. Park, J. Lee, Y. J. Song, S. Lee and J.-H. Park, *Adv. Mater.*, 2016, **28**, 6711–6718.
- K. S. Kim, Y. J. Ji, K. H. Kim, S. H. Choi, D. H. Kang, K. Heo, S. J. Cho, S. M. Yim, S. J. Lee, J. H. Park, Y. S. Jung and G. Y. Yeom, *Nat. Commun.*, 2019, **10**, 1–10.
- K. S. Novoselov, A. K. Geim, S. V. Morozov, D. Jiang, Y. Zhang, S. V. Dubonos, I. V. Grigorieva and A. A. Firsov, *Science*, 2004, **306**, 666–669.
- M. Nonnenmacher, M. P. O'Boyle and H. K. Wickramasinghe, *Appl. Phys. Lett.*, 1991, **58**, 2921–2923.
- G. Kresse and J. Furthmüller, *Comput. Mater. Sci.*, 1996, **6**, 15–50.